Conductance features in point contact Andreev reflection spectra

2009 J. Phys.: Condens. Matter 21 095701

(http://iopscience.iop.org/0953-8984/21/9/095701)

J. Phys.: Condens. Matter **21** (2009) 095701 (8pp) doi:10.1088/0953-8984/21/9/095701

Conductance features in point contact Andreev reflection spectra

V Baltz[1,3], A D Naylor[1], K M Seemann[1], W Elder[1], S Sheen[1], K Westerholt[2], H Zabel[2], G Burnell[1], C H Marrows[1] and B J Hickey[1,4]

[1] School of Physics and Astronomy, University of Leeds, Leeds LS2 9JT, UK
[2] Department of Physics, Ruhr-University Bochum, D-44780 Bochum, Germany

E-mail: vincent.baltz@cea.fr and b.j.hickey@leeds.ac.uk

Received 29 August 2008, in final form 15 January 2009
Published 4 February 2009
Online at stacks.iop.org/JPhysCM/21/095701

Abstract
Point contact Andreev reflection (PCAR) spectroscopy is a common technique for determining the spin polarization of a ferromagnetic sample. The polarization is extracted by measuring the bias dependence of the conductance of a metallic/superconducting point contact. Under ideal conditions, the conductance is dominated by Andreev reflection and the Blonder–Tinkham–Klapwijk (BTK) model can be used to extract a value for the polarization. However, PCAR spectra often exhibit unwanted features in the conductance that cannot be appropriately modelled with the BTK theory. In this paper we isolate some of these unwanted features and show that any further extraction of the spin polarization from these non-ideal spectra proves unreliable. Understanding the origin of these features provides an objective criterion for rejection of PCAR spectra unsuitable for fitting with the modified BTK model.

(Some figures in this article are in colour only in the electronic version)

1. Introduction

Measuring the spin polarization of a current in various electrical regimes [1] is a key step towards the understanding and further implementation of more sensitive devices based on spin injection, spin filtering, giant magnetoresistance or tunnel magnetoresistance (TMR) [2]. Among the different experimental techniques available are point contact Andreev reflection (PCAR) [3, 4], the Tedrow and Merservey method [5], TMR experiments [6], and spin resolved photoemission [7].

In PCAR experiments a point contact is formed between a superconductor and a ferromagnet. The spin polarization of the current incident at the point contact can then be determined by fitting the bias dependence of the conductance with the modified Blonder–Tinkham–Klapwijk (BTK) theory [4]. In its simplest form the model incorporates four parameters; the superconducting energy gap Δ, the spin polarization P, a broadening parameter ω and a parameter that describes the transparency of the interface, Z [3, 4, 8, 9]. Further parameters have been introduced into the model to account for additional effects including the presence of a series resistance [9], a thin superconducting proximity layer in the sample [4] and a finite quasi-particle lifetime in the vicinity of the contact [10–12]. The interdependence of the spin polarization P and the interface parameter Z are often used to extract the spin polarization of the ferromagnet. Despite a seemingly oversimplified description of the point contact system [11–14] the modified BTK model provides excellent fits to conductance spectra and the values of polarization extracted are in agreement with complementary techniques [3, 4, 8, 9, 15].

However, in recent years it has become increasingly clear that great care must be taken when interpreting the fit parameters from PCAR data [8, 9, 16]. The presence of the film resistance in series with the point contact can distort the conductance data and modify the point contact parameters that are extracted from the fit [9]. Due to the large number of free fitting parameters, and the interdependence between them, fits to PCAR spectra can be degenerate [8]. The inclusion of further parameters into the model increases the degeneracy and can prevent the determination of a unique value for the spin polarization. Further to these problems, conductance spectra often contain features that cannot be modelled with

[3] Present address: SPINTEC (URA 2512 CNRS/CEA), 17, avenue des Martyrs, 38054 Grenoble, France.
[4] Author to whom any correspondence should be addressed.

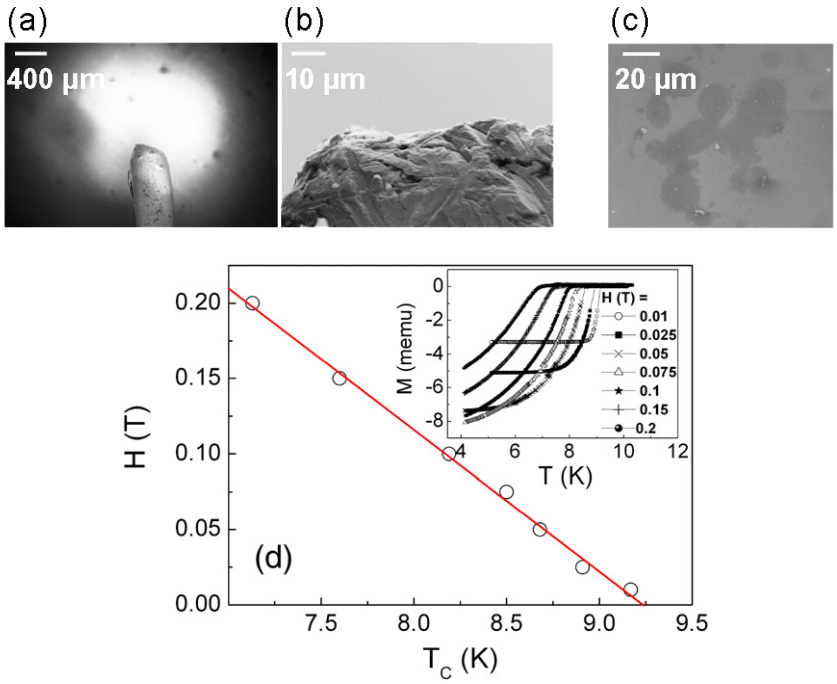

Figure 1. Scanning electron microscopy image of (a) and (b) a typical Nb tip and (c) holes resulting from contacts between such a tip and a Au/Co_2MnGe/Au thin film. (d) shows the dependence of the magnetic field, H, as a function of the critical temperature, T_C, of the Nb tip, as deduced from the dependences of the magnetization of the tip, M, with the temperature, T, for different external magnetic field, H (shown in the inset). The red line in (d) is a fit to the data in the Ginzburg–Landau limit.

the modified BTK theory. These features occur in a variety of forms and can result in conductance spectra that vary significantly from the ideal case described by the modified BTK model. Without understanding the origin of these features it is difficult to decide what should be done; often these spectra are ignored and discarded from further analysis. This process of discarding inappropriate curves is ambiguous as there is no well defined criterion for rejection.

In this paper, we highlight specific features in the conductance spectra that can render the data unsuitable for fitting with the modified BTK model. After providing an example of an ideal spectrum we isolate some of these unwanted features in order to understand their origin, and show that any further extraction of the spin polarization proves unreliable. For each feature we suggest an experimental technique for removal from subsequent spectra. Understanding the origin of these features provides an objective criterion for the rejection of PCAR spectra that cannot be appropriately modelled with the modified BTK theory. Finally, we illustrate that after rejection of unsuitable spectra we were able to accurately measure the spin polarization in some 3d transition metals (Ni, Co, Fe), alloys (FePt and FePd) and inter-metallic Heusler alloys (Co_2MnGe and Co_2MnSn).

2. Experimental procedures

A variety of samples were used to isolate some of the unwanted features in conductance spectra. Thin films of Fe, Co and Ni were DC sputtered on oxidized silicon substrates. The alloys FePt and FePd were prepared via the growth technique described in [17]. Measurements were also completed on two inter-metallic Heusler compounds, Co_2MnGe and Co_2MnSn. The growth and characterization of these samples is detailed in [18].

The superconducting tips were prepared from commercial 99.9% pure Nb wires with a diameter of 500 μm. The tips were sharpened by a simple cut at grazing incidence. Surprisingly and as detailed in the literature, the preparation method of the tip is not crucial [8]. Notably, the simple cut of some brittle metals can result in tips atomically sharp apices [19]. Scanning electron microscopy images of a typical tip are shown in figures 1(a) and (b). They reveal that the extremity of the tip is of tens of microns wide and is terminated by some micron size apices. Due to the pressure necessary to establish a stable low-resistance contact, the tip has to be squashed against the sample [8, 9] and the trace left by the tip, after a contact has been made is around 20 μm, as shown in figure 1(c).

In order to further characterize our tips, vibrating sample magnetometry measurements of the tip magnetization with temperature and magnetic field were performed. They are shown in the inset of figure 1(d). The critical temperature, T_C with the magnetic field, H is plotted in figure 1(d). The critical temperature at $H = 0$ was 9.25 K. Using Ginzburg–Landau theory we were then able to determine a value for the superconducting energy gap at 4.2 K, $\Delta_{Nb} = 1.42$ meV, the electron mean free path, $\lambda = 19$ nm, and the resistivity of the tip in the normal state, $\rho = 6.1$ $\mu\Omega$ cm [20–24]. The contact radius, a, can then be calculated using the Sharvin formula [25] $a = [(4\rho\lambda)/(3\pi R)]^{1/2}$. A typical contact resistance yields a contact size of $\sim$10 nm. This contact size is clearly smaller than the size of the tip footprint shown in figure 1(c) suggesting

the presence of multiple nano-size contacts in parallel [8, 9]. We note the product of the mean free path times the resistivity as deduced for the Nb tip is of the order of 1 fΩ m^{-2}, which is also the right approximation for metallic materials [26]. We can thus safely use the above deduced parameters in order to estimate the size of the contact between the Nb tip and the metallic materials that we have studied.

PCAR measurements were performed at 4.2 K in a liquid He bath cryostat using the Nb wire attached either to a standard spring-loaded rod driven by a micrometer screw or to a piezoelectric mechanism [3, 4, 8, 9, 15, 16]. Two spring-loaded macroscopic pads made of brass contact the surrounding sheet film of the sample. A bias voltage was applied across the point contact and the differential conductance was recorded via a four-probe technique, as depicted in figure 2 of [15]. For the Heusler alloys, we note that the bias voltage is applied between the contact on the mesa and the surrounding continuous film; the current is then driven vertically through the mesa and thus across the material to be studied. Since the surrounding film is made of a conductive metal, gold, the effect of the spreading resistance is minimized [8, 9]. AC lock-in detection with a 100 μV amplitude and a 5.1 kHz frequency was used for the differential conductance measurements.

3. Results and discussions

Before discussing the features that can render PCAR spectra unsuitable for fitting we give an example of an ideal spectrum. Figure 2(a) shows a conductance curve from a contact between a Nb tip and a Co thin film. The peak centred around zero bias is the signature of Andreev reflection [3, 4], while the dip within the peak is characteristic of scattering at the interface. At high bias the conductance becomes independent of the applied voltage and levels off at a constant value.

The red dashed line in figure 2(a) is a fit to the raw data with the modified BTK model proposed in [4, 8]. We use the parameters in the same way as [8]. The fit yields a broadening parameter, ω of (0.69 $\pm$ 0.02) meV, an unrealistic superconducting gap, $\Delta_{\rm raw}$, of (1.94 $\pm$ 0.01) meV, a barrier strength, Z, of (0.23 $\pm$ 0.01), and a current spin polarization, P, of (0.44 $\pm$ 0.01). Overestimations of the superconducting gap are commonly ascribed to spreading resistances, $R_{\rm Spreading}$ [9, 17]. Spreading resistances are manifest in PCAR data when the resistance of the point contact is comparable to the resistance of the surrounding film [8, 9, 17]. The necessity for a spreading resistance correction is determined by the ratio of the point contact resistance to the film resistance. When the point contact resistance is an order of magnitude larger than the film resistance, for instance in the presence of a highly conductive substrate, the series resistance becomes negligible. The spreading resistance can vary between contacts to the same film as each individual point contact is formed at a unique position relative to the two electrode contacts to the film. In this case the spreading resistance was estimated by rescaling the fitted gap from the raw data to the one that we have previously measured (section 2): $\Delta_{\rm Nb}G_{\rm Corrected} = \Delta_{\rm raw}G_{\rm raw}$ and $(1/G_{\rm raw}) = (1/G_{\rm Corrected} + R_{\rm Spreading})$, with $G_{\rm raw}$ the value of the raw conductance for eV $= \Delta_{\rm raw}$. The red solid line

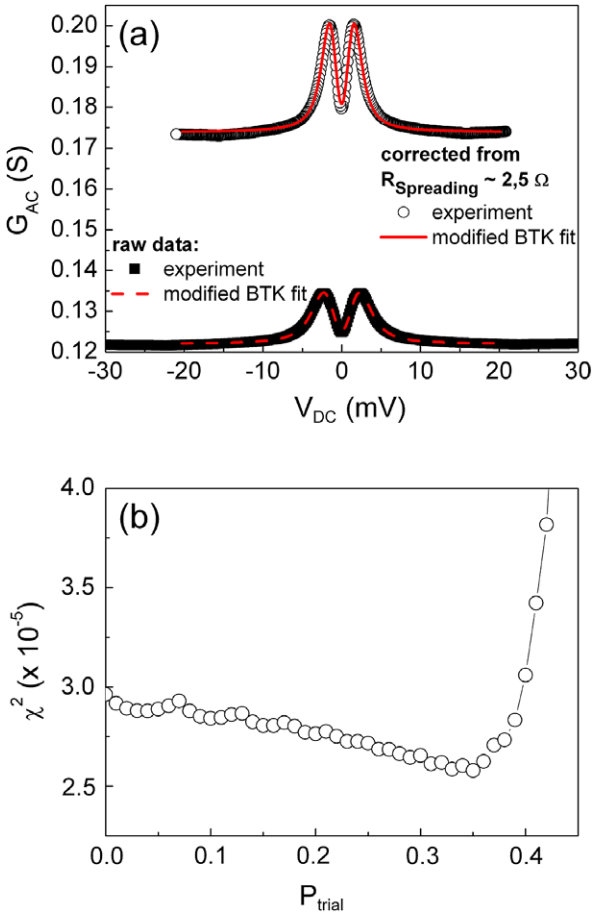

Figure 2. (a) Conductance data from contact between a Co/Nb point contact before and after correction from a spreading resistance. The red dashed line is a fit to the raw data using the modified BTK model proposed in [4, 8]. The fitting parameters were $\omega = (0.69 \pm 0.02)$ meV, $\Delta = (1.83 \pm 0.02)$ meV, $Z = (0.31 \pm 0.01)$, and $P = (0.41 \pm 0.01)$. The red solid line is a fit to the corrected data. The fitting parameters were $\omega = (0.49 \pm 0.02)$ meV, $\Delta = (1.36 \pm 0.05)$ meV, $Z = (0.38 \pm 0.02)$, and $P = (0.35 \pm 0.01)$. (b) χ^2 analysis of the corrected data shown in (a).

in figure 2(a) is a fit to the data corrected for a spreading resistance of approximately 2.5 Ω. We now obtain: $\omega = (0.49 \pm 0.02)$ meV, $\Delta = (1.36 \pm 0.05)$ meV, $Z = (0.38 \pm 0.02)$, and $P = (0.35 \pm 0.01)$.

It is well known that fits to PCAR data can be degenerate due to the large number of fitting parameters and the inter-relationships between them. To examine the degeneracy of our fits in polarization P, we follow the approach of Bugoslavsky *et al* [8]. Constraining a trial polarization, we fit with Z, Δ and ω as free parameters and calculate the χ^2 statistic for that fit. A plot of χ^2 against $P_{\rm Trial}$ for the data in figure 2(a) is shown in figure 2(b). There is a well defined minimum in χ^2 ($P_{\rm Trial}$) indicating a unique best fit for $P = 0.35$. In addition to the known degeneracy for low values of P, additional parameters in the model will result in increased degeneracy of solutions and should be avoided where possible.

A series of point contacts were formed between a Nb tip and a Co thin film, and the conductance was measured for each contact. In figures 3(a)–(d), the fitting parameters

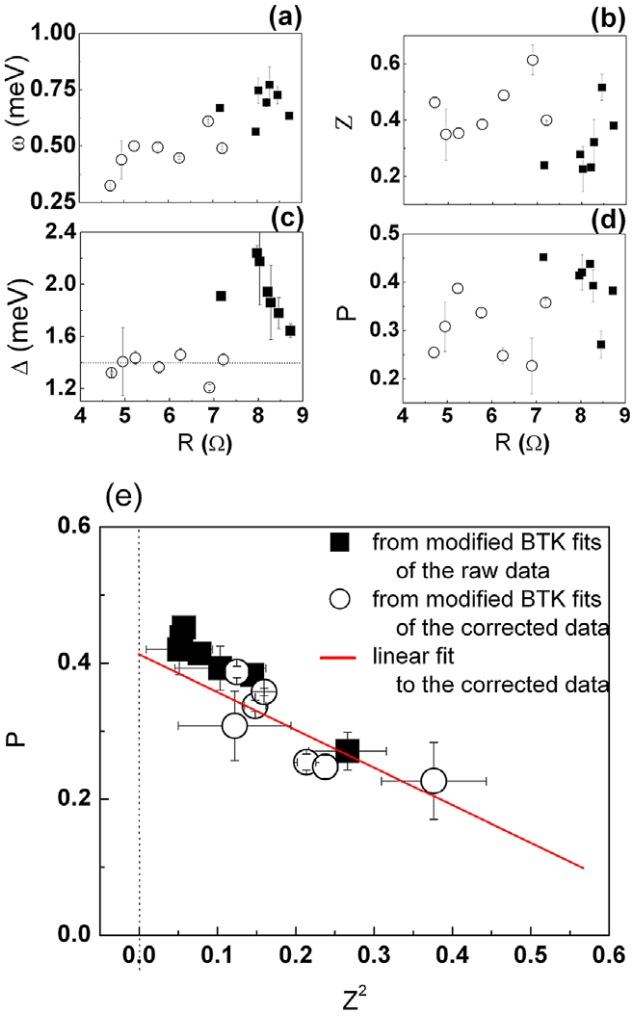

Figure 3. (a)–(e) Modified BTK fitting parameters versus contact resistance, from a series of point contacts. The line in (c) accounts for the bulk value of Δ. (e) Corresponding dependence of the polarization, P, with the square of the barrier strength, Z^2. The red solid line is a linear fit of the data.

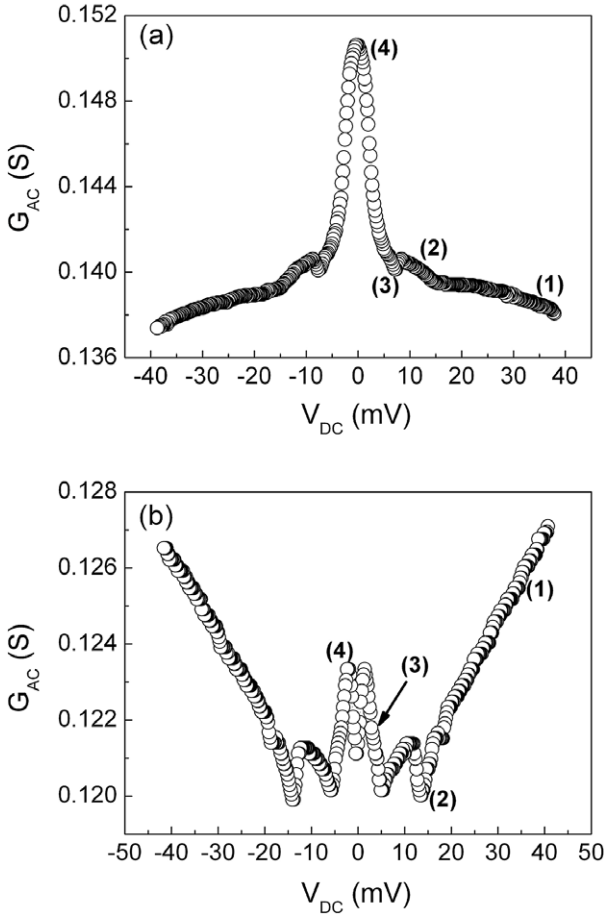

Figure 4. Conductance spectra for contacts between (a) a Ni film and Nb tip, and (b) a Au/Co2MnGe/V film and Nb tip. The features of relevance are numbered within the plots.

of the resulting set of conductance curves are plotted as a function of the contact resistance, R. Figure 3(a) shows the dependence of the broadening parameter, ω [4, 8]. This parameter includes all processes, both thermal and a-thermal, that contribute to a broadening of the conductance spectra. The thermal broadening results from the smearing of the Fermi–Dirac distribution function at non-zero temperatures. There are several mechanisms that contribute to an a-thermal spectral broadening. These include the effect of a varying quasi-particle lifetime in the vicinity of the contact [10–12], interface scattering [8] and some deficiencies in the BTK model [27, 28]. Distinguishing between these forms of broadening is difficult, and beyond the scope of this work, but we note that the effect of a finite quasi-particle lifetime is probably negligible in our case since this has been shown to be significant only close to phase transitions (ferromagnetic/paramagnetic [12] or superconducting/normal [11]). The correlation between the contact resistance and ω shown in figure 3(a) suggests that interface scattering contributes to the broadening for these contacts.

Figure 3(b) shows the relationship between the contact resistance and the interface parameter Z. As previously observed, there is no clear correlation between the two. This has been ascribed to the fact that the contact resistance is determined mainly by the size of the contact rather that its cleanness [4]. Figure 3(d) shows that the current spin polarization does not depend on the contact resistance in any obvious fashion. Rather note that, as expected, the fitted spin polarization seems to systematically depend on the barrier strength Z. Figure 3(e) thus shows the dependence of the polarization as a function of the square of the barrier strength, Z^2. The solid line in figure 3(e) is a linear fit to the data. The relevant value of the polarization is usually achieved from an extraction to the regime of perfect interface transparency, $Z = 0$. From the interdependence of P and Z for repeated contacts, and in the optimum conditions, i.e. without unwanted features, we could extract the spin polarization of the current. Here, as an example and from figure 3(e), we find $P = (0.41 \pm 0.03)$ for cobalt, in good agreement with the literature [4, 15].

3.1. Detrimental features

As can be seen in figure 4, conductance spectra can vary significantly from the ideal shape shown in figure 2(a). We note that such curves are typical of what we often observed

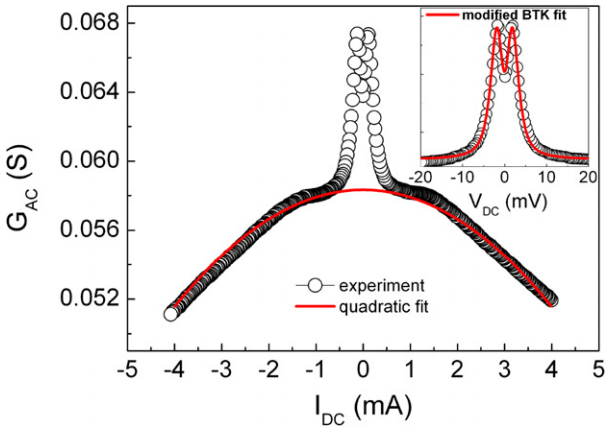

Figure 5. Current dependence of the conductance for a Ni film—Nb tip point contact. The red solid line is a quadratic fit to the high bias voltage data. The inset shows a zoom of the conductance versus bias voltage data after correction from the quadratic contribution. The red solid line in the inset is a fit to the data using the modified BTK model proposed in [4, 8]. The fitting parameters were $\omega = (0.7 \pm 0.1)$ meV, $\Delta = (1.73 \pm 0.24)$ meV, $Z = (0.34 \pm 0.09)$, and $P = (0.33 \pm 0.04)$.

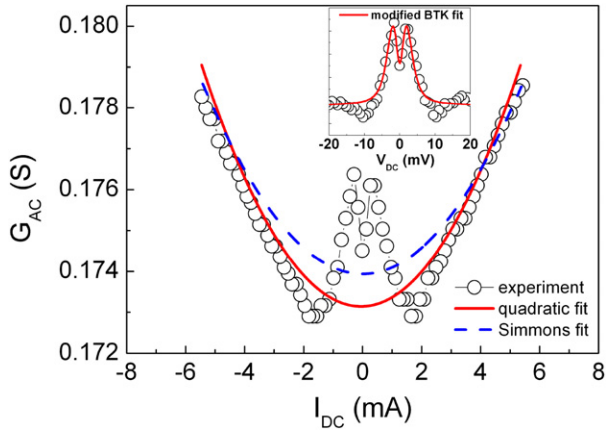

Figure 6. Current dependence of the conductance across a Au/Co2MnGe/V film-Nb tip point contact. The red solid line and the blue dashed line are respectively a quadratic fit and a Simmons fit to the data for the large values of voltages. The inset shows a zoom of the corresponding dependence of the conductance with the point contact bias voltage after correction from the quadratic background. The red solid line in the inset is a fit to the data using the modified BTK model proposed in [4, 8]. The fitting parameters were $\omega = (1 \pm 0.25)$ meV, $\Delta = (0.7 \pm 0.2)$ meV, $Z = (0.4 \pm 0.7)$, and $P = (0.4 \pm 0.2)$.

when collecting a series of PCAR spectra. In both figures 4(a) and (b) one can distinguish the low bias signature previously ascribed to Andreev reflection (numbered as (4) within the figure). In figure 4(b), the central dip surrounded by two shoulders suggests a large barrier strength, Z. The absence of any dip at zero bias in the case of figure 4(a) suggests either a low value of Z or more likely, that the contact is measured in the extreme thermal regime [29]. In both figures the conductance does not plateau at high bias as observed in the ideal case. In figure 4(a) the conductance decreases with increasing bias, while the opposite case is observed in figure 4(b). For both measurements, we also observe some additional dips in the curve and sharp deviations of slope (features numbered 2 and 3).

In order to understand the origin of these unwanted features we have attempted to isolate them in single conductance curves.

3.1.1. Joule heating. Figure 5 shows the feature labelled (1) in figure 4(a), i.e. a reduction of the conductance with increasing current. Such a reduction may result from Joule heating, thus yielding the parabolic shape seen in figure 5. Joule heating is inversely proportional to the point contact resistance, however the Joule heating in the film is directly proportional to the series resistance. Thus the Joule heating does not scale directly with the total resistance; rather it becomes increasingly prominent in the presence of a small point contact resistance and a high series resistance. A correction for the quadratic background (as indicated by the red solid line in figure 5) still allows for an approximate fitting with the modified BTK model, as shown in the inset of figure 5. Although the corrected fit yields plausible parameters it is achieved at the expense of an additional fitting parameter and hence an increase in degeneracy. This artefact therefore reduces the likelihood of a unique fit to the data, and consequently the ability to extract a unique value for the spin polarization.

Spectra exhibiting this feature should therefore be rejected from further analysis. Given the ease with which PCAR spectra are obtained, the contact can be modified or re-formed until an optimum curve is achieved. This artefact could be removed experimentally by a slight withdrawal of the tip. This decreases the contact area and increases the contact resistance, reducing the Joule heating. Alternatively an entirely new contact can be formed.

3.1.2. Tunnel barriers. The feature labelled (1) in figure 4(b) can be observed in figure 6; an increase in conductance with increasing current. The shape of the curve, which is consistent with tunnelling through a small barrier, can be fitted with a simple quadratic law. Such a barrier may arise from oxidation of either the tip or the sample, or as a result of some barrier formation within the sample itself. In this case the surface is capped with a thin gold layer to avoid sample surface oxidation, and we can rule out the presence of a barrier within the sample itself as this feature is not present in all spectra collected from the film. Here it is likely that a native oxide, possibly with composition NbO_x/Nb_2O_{5-y} [30] forms on the Nb tip, resulting in a tunnel barrier. The quality of this barrier is expected to be very poor, with structural inhomogeneities and pinholes. Our attempts to fit the experimental data with a more accurate Simmons law [31] which still assumes an homogeneous barrier (see blue dashed line in figure 6) resulted in a set of implausible parameters: a barrier thickness of (2 ± 3) nm, a barrier height of (0.1 ± 3) meV and a contact area of $(9.06 \pm 0.04) \times 10^{-8}$ m^2.

After correcting for the quadratic background the data can still be fitted with the modified BTK model, as shown in the

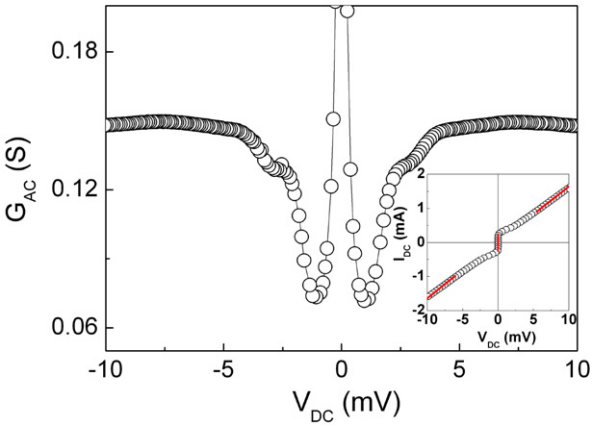

Figure 7. Conductance spectra for a contact between a Nb film and Nb tip. The inset shows the corresponding current versus bias voltage measurement. The lines in the inset are guides to the eye: the vertical line indicates the superconducting transport regime and the linear lines indicate the ohmic transport regime.

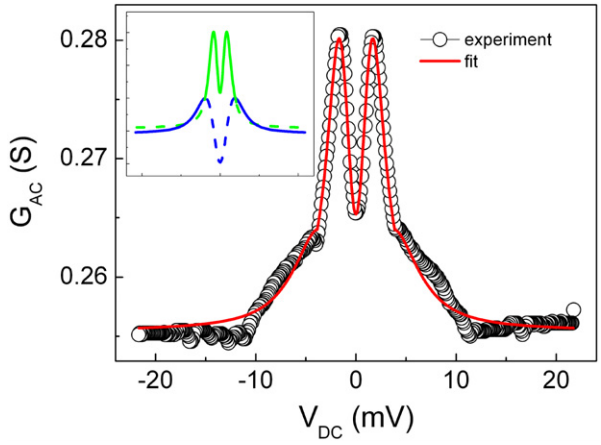

Figure 8. (a) Conductance curve from a point contact between a Ni film and a Nb tip. The red solid line is a fit to the data using the modified BTK model proposed in [4, 8]. For $|V| < 4$ mV, the fitting parameters were $\omega = (0.56 \pm 0.06)$ meV, $\Delta = (1.35 \pm 0.11)$ meV, $Z = (0.25 \pm 0.08)$, and $P = (0.43 \pm 0.03)$, and for $|V| > 4$ mV, the fitting parameters were $\omega = (1.25 \pm 0.05)$ meV, $\Delta = (1.8 \pm 0.37)$ meV, $Z = (0.34 \pm 0.21)$, and $P = (0.47 \pm 0.08)$. The inset shows the corresponding two loops over the whole range of V.

inset of figure 6. This correction requires the introduction of a further parameter into the model and consequently increases the fit degeneracy. As a result, fits to the corrected data are largely degenerate and the resulting parameters exhibit large errors: $\omega = (1 \pm 0.25)$ meV, $\Delta = (0.7 \pm 0.2)$ meV, $Z = (0.4 \pm 0.7)$, and $P = (0.4 \pm 0.2)$. A unique set of solutions can no longer be achieved and thus the spin polarization cannot be determined.

It is thus essential to ensure such barriers are not present in the point contact system. This may involve capping samples to prevent oxidation, preparing the tip immediately before introduction into the cryostat and the growth of all sample layers *in situ* where possible. In this case, since the native oxide layers form slowly (up to three days [32]) and reach only a few nanometres [30], they are easily removed by crushing the tip into the surface. We note that this may cause some structural damage to the sample that may in turn lead to a reduction of P for certain materials. In this case the next contact should be formed at another location on the film and the value for P regarded as a lower limit. It may also be possible to remove the oxide by running a large current through the tip in order to break down the barrier [33].

3.1.3. Critical superconducting current. The dips in conductance observed in figures 4(a) and (b) (numbered (3) and (2), respectively) have already been studied in the literature. They were ascribed to the finite resistance of the superconductor above the critical current when the contact is no longer in the ballistic limit. More detailed information on that point can be found in [29]. We remark that the dip as observed in the conductance spectrum of figure 6 might as well be associated with the current at the contact reaching the critical current, as discussed in the previous paragraph. Shown in figure 7 of this manuscript is a conductance measurement of one of our Nb tips in contact with a Nb film, along with its corresponding $I(V)$, shown in the inset. Two dips are visible in the conductance, but as there are only superconductors in this point contact system it is evident that these dips are not related to the Andreev reflection process, which requires both a superconductor and a normal metal. The presence of these dips is not predicted by the original BTK theory. Dips in the conductance can also arise when Cooper pairs from the superconductor leak into the metal [4]. For non-ferromagnetic samples, distinguishing between these two effects is non-trivial. As discussed in [29] fitting a spectrum exhibiting these dips with the modified BTK model can lead to unreliable fit parameters. This feature can be removed by increasing the total contact resistance, and thus reducing the area of the contact, as shown in figure 2 of [29].

3.1.4. Multiple contacts. Figure 8 shows an artefact similar to features (2) and (3) in figures 4(a) and (b), respectively. The data resembles two conventional PCAR spectra with very different parameters superimposed, as illustrated in the inset of figure 8. There are two approaches to fitting such a curve. The first involves defining a model that calculates the conductance of two point contacts in parallel, while the second performs a single fit with the modified BTK model to specific regions of the data. For the curve shown in figure 8 this would involve a fit to the low bias peaks for one contact, and a fit to the high bias data for the second. Both of these techniques double the number of parameters required to fit the conductance data and are consequently largely degenerate. An accurate value for the polarization cannot then be determined. We note that to achieve such an extreme variation in slope requires two contacts with very different parameters, particularly Δ. This may explain why such curves are relatively infrequent despite the continual presence of multiple contacts. Experimental removal of this feature involves re-configuring the tip apex—either by re-cutting the tip or crushing the tip into the sample. In conclusion, multiple contacts that display a large variation in parameters prevent an accurate extraction of the polarization.

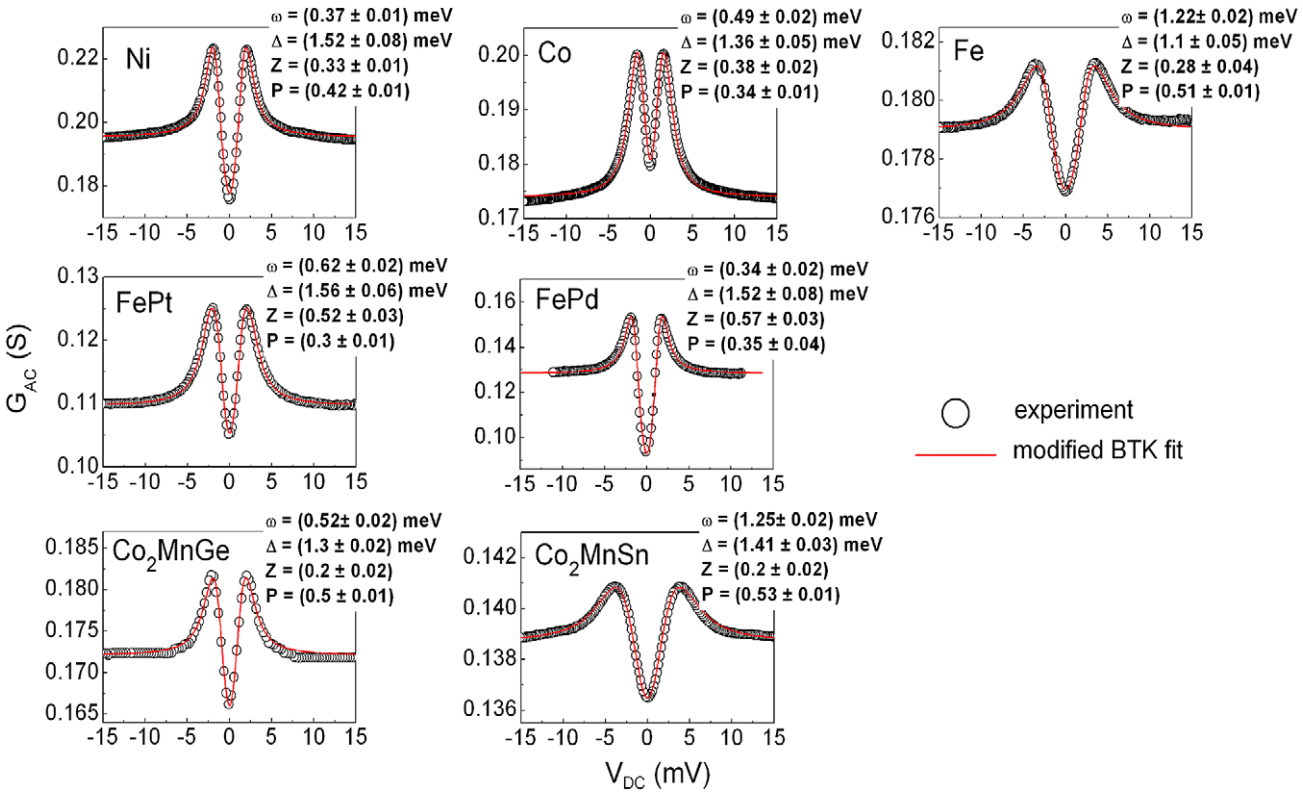

Figure 9. Examples of optimum spectra from measurements on a variety of materials with a Nb tip. The solid lines are fits to the data

3.2. Optimal spectra

All the features described above are detrimental to the extraction of the spin polarization. Contacts that exhibit such features in the conductance data should therefore be re-formed. Only spectra suitable for fitting with the modified BTK model are then included in the further analysis used to extract the spin polarization. Figure 9 shows some examples of optimum spectra for various materials. By repeating the fitting procedure described in the introduction of section 3, we could achieve the P versus Z^2 plot and extract the spin polarization, as shown in figure 10.

We validated our procedure by measuring a set of 3d transition metals (Ni, Co, Fe) with well known spin polarization. Two samples of Ni and Fe have been fabricated and measured in order to qualitatively estimate the spread in the polarization (∼3%–6%) between samples. The values are in good agreement with the literature [3, 4, 15, 16].

Thus, with some confidence we have measured several alloys. Measurements on FePt, and FePd for different chemical ordering parameters allowed us to further investigate and compare the polarization of the current in different transport regimes. We could thus demonstrate the key role played by the spin dependent scattering probability in the polarization of the current, which is the subject of [17]. Two potentially half-metallic Heusler alloys were also measured. The values of spin polarization extracted were significantly lower than the theoretically predicted 100%, but in agreement with previous PCAR experiments [34]. This reduction in spin polarization is attributed to disorder within the Heusler compound. Band

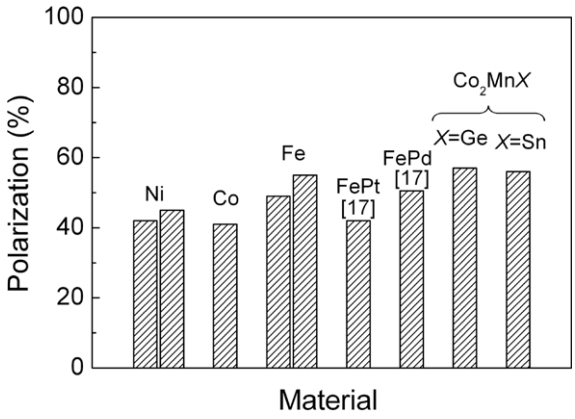

Figure 10. Values of the current spin polarization in various materials, as measured by Andreev reflection with our experimental setup.

structure calculations taking into account antisite disorder and atomic interchange, have shown that disorder within the crystal can destroy the half-metallicity and significantly reduce the spin polarization [35–37].

4. Conclusion

We have studied the conductance versus bias voltage characteristics of point contacts between a superconducting tip and thin films. We have shown that some unwanted features can appear in PCAR spectra that render the data unsuitable for

fitting with the modified BTK theory. We have isolated these features in conductance spectra in order to understand their origin. We believe that they are ascribed to either (i) Joule heating, (ii) the oxidation of the tip, (iii) the tip going normal at low bias voltage due to its reduced size, and (iv) multiple contacts in parallel. An experimental approach is suggested for the removal of each feature. In some cases it is still possible to fit with the modified BTK model, however correcting the data requires the introduction of further parameters and hence increases the degeneracy. Consequently these curves should be rejected from further analysis. The unwanted features are not present in all spectra; contacts providing unsuitable data can simply be re-formed or modified until the optimum shape of spectrum is achieved. Understanding the origin of these features legitimizes the rejection of curves that are unsuitable for fitting with the modified BTK model. Finally, we illustrated our procedure by showing examples of measurements of optimum spectra for selected materials, including (i) some usual 3d transition metals (Ni, Co, Fe) which allowed us to validate our procedure and (ii) some less commonly studied materials which are potentially interesting materials for use as current spin polarizers: (FePt, FePd) alloys, and inter-metallic Heusler alloys (Co_2MnGe, Co_2MnSn).

Acknowledgments

The authors acknowledge A T Hindmarch, M Ali, and J Turton for their help with the upgrade of the point contact experiment. A S Walton and C S Allen are thanked for the SEM images. Work supported in part by the European Community's Marie Curie actions (Research Training Networks) under contract MRTN-CT-2003-504462, ULTRASMOOTH, and by the EPSRC through the Spin@RT consortium.

References

[1] Mazin I I 1999 *Phys. Rev. Lett.* **83** 1427
[2] Prinz G A 1998 *Science* **282** 1660
[3] Soulen R J Jr *et al* 1998 *Science* **282** 85
[4] Strijkers G J, Ji Y, Yang F Y, Chien C L and Byers J M 2001 *Phys. Rev.* B **63** 104510
[5] Tedrow P M and Meservey R 1971 *Phys. Rev. Lett.* **26** 192
[6] Verduijn E A and Westerholt K 2006 *J. Appl. Phys.* **99** 084502
[7] Ristoiu D *et al* 2000 *Europhys. Lett.* **49** 624
[8] Bugoslavsky Y *et al* 2005 *Phys. Rev.* B **71** 104523
[9] Woods G T, Soulen R J, Mazin I and Nadgorny B 2004 *Phys. Rev.* B **70** 054416
[10] Dynes R C, Narayanamurti V and Garno J P 1978 *Phys. Rev. Lett.* **41** 1509
[11] Mukhopadhyay S, Raychaudhuri P, Joshi D A and Tomy C V 2007 *Phys. Rev.* B **75** 014504
[12] Mukhopadhyay S, Dhar S K and Raychaudhuri P 2008 *Appl. Phys. Lett.* **93,** 102502
[13] Pérez-Willard F *et al* 2004 *Phys. Rev.* B **69** 140502R
[14] Stokmaier M, Goll G, Weissenberger D, Sürgers C and Löhneysen H v 2008 *Phys. Rev Lett.* **101** 147005
[15] Soulen R J Jr *et al* 1999 *J. Appl. Phys.* **85** 4589
[16] Kant C H *et al* 2002 *Phys. Rev.* B **66** 212403
[17] Seemann K M *et al* 2007 *Phys. Rev.* B **76** 174435
Seemann K M, Hickey M C, Baltz V, Hickey B J and Marrows C H 2009 unpublished
[18] Westerholt K *et al* 2005 *Half-Metallic-Alloys Fundamental and Applications* (New York: Springer)
[19] Guckenberger R, Hartmann T, Wiegräbe W and Bauneister W 1995 *Scanning Tunneling Microscopy II* ed R Wiesendanger and H J Güntherodt (Berlin: Springer)
[20] de Gennes P G 1966 *Superconductivity of Metals and Alloys* (New York: Benjamin)
[21] Potenza A and Marrows C H 2005 *Phys. Rev.* B **71** 180503
[22] Bardeen J, Cooper L N and Schrieffer J R 1957 *Phys. Rev.* **108** 1175
[23] Hauser J J, Theuerer H C and Werthamer N R 1966 *Phys. Rev.* **142** 118
[24] Ashcroft N and Mermin N 1976 *Solid State Physics* (New York: Saunders)
[25] Sharvin Y V 1965 *Zh. Eksp. Teor. Fiz.* **48** 984
Sharvin Y V 1965 *Sov. Phys.—JETP* **21** 655 (Engl. Transl.)
[26] Bass J and Pratt W P 2007 *J. Phys.: Condens. Matter* **19** 183201
[27] Kant C H 2005 Probing spin polarization: point contacts and tunnel junctions *PhD Thesis* from the Technische Universiteit Eindhoven http://alexandria.tue.nl/extra2/200510447.pdf
[28] van Son P C, van Kempen H and Wyder P 1988 *Phys. Rev.* B **37** 5015
[29] Sheet G, Mukhopadhyay S and Raychaudhuri P 2004 *Phys. Rev.* B **69** 134507
[30] Halbritter J 1985 *IEEE Trans. Magn.* **21** 2
[31] Simmons J G 1963 *J. Appl. Phys.* **34** 1793
[32] Rowell J M, Gurvitch M and Geerk J 1981 *Phys. Rev.* B **24** 2278
[33] Cole A, Hickey B J, Hase T P A, Buchanan J D R and Tanner B K 2004 *J. Phys.: Condens. Matter* **16** 1197
[34] Rajanikanth A, Kande D, Takahashi Y K and Hono K 2007 *J. Appl. Phys.* **101** 09J508
[35] Ishida S, Kashiwagi S, Fujii S and Asano S 1995 *Physica* B **210** 140
[36] Picozzi S, Continenza A and Freeman A 2004 *Phys. Rev.* B **69** 094423
[37] Grabis J, Bergmann A, Nefedov A, Westerholt K and Zabel H 2005 *Phys. Rev.* B **72** 024437